

UNCONDITIONALLY STABLE, EFFICIENT AND ROBUST NUMERICAL SIMULATION OF ISOTHERMAL COMPOSITIONAL GRADING BY GRAVITY

XIAOLIN FAN, ZHONGHUA QIAO, AND SHUYU SUN*

ABSTRACT. The gravitational force has been considered as one of the most important factors leading to composition variation of multicomponent chemical species mixture in many industrial processes and natural phenomena. This has been largely studied through experimental and numerical modeling, especially in chemical processes and petroleum reservoir engineering. The modeling and simulation of dynamical process of composition variation under gravity is fundamentally important to understand the evolutionary process of petroleum reservoir formation and initial state. This work presents the dynamical modeling of composition variation in the framework of the modified Helmholtz free energy coupling with the realistic equations of state. An efficient, easy-to-implement, thermodynamically consistent, and robust numerical scheme is proposed for the dynamical model. This scheme is rigorously proved to be unconditionally stable. The implementation is straightforward based on the single-component system and is not required to choose a reference species for multicomponent fluids. For the multicomponent system of huge number of species, the proposed scheme allows to numerically compute the system of partial differential equations in a random order, which is called "unbiased scheme" in this work. The current scheme is computationally efficient and saves computer memory. Several numerical examples are conducted to verify the properties of the scheme.

1. INTRODUCTION

In the petroleum reservoir engineering, an accurate calculation of the initial distribution of hydrocarbon mixture in the reservoir is one of the necessary and essential preliminary conditions for a successful production optimization plan development; it also indicates the reservoir connectivity and design suitable recovery schemes, in particular if the compositional variation results in changing phase behavior with depth. There are numerous observed factors that influence the distribution of components in the reservoir among which gravity plays one of the most significant roles, in particular for the thermodynamic systems that extend over a large domain or are near the critical point (see [36, 41, 49, 54] and references therein).

Due to its importance, there has been a great deal of study on mathematical modeling and numerical simulation of compositional grading phenomenon in literature. Gibbs [13] as the first researcher formulated the general equilibrium conditions for multicomponent ideal fluids mixture under isothermal circumstances considering the gravity effect. Lewis and Randall in [28] then derived the general differential equations for the distribution of non-reacting ideal fluids under the effect of gravity at equilibrium. Following Lewis and Randall, Muskat in 1930 [37] analyzed the the equations and obtained barometric formula for ideal incompressible fluids in a gravity field and also gave the numerical results for a binary ideal solution of liquids. Sage et al. in [49] derived the general conditions for reversible process of liquid-gas two-phase hydrocarbon mixture systems at thermodynamic equilibrium in a uniform gravitational field and discussed the composition variation with elevation. The gravity effect has also been studied for fluids near the gas-liquid critical point by Moldover et al. in [34]. In [31], Lira-Galeana et al. proposed a continuous thermodynamic framework with an equation of state to calculate the compositional grading in hydrocarbon reservoirs and they utilized the method of moments to analytically formulate segregation characteristics by gravity force of the heavy fractions of the oil. With the the theory for compositional variation in a gravitational field being developed, it has been applied the the compositional variation in the gravitational field to analyze the gas-oil ratio, saturation point and condensate gas ratio calculations for some real reservoirs (see [8, 15, 32, 35, 43, 50] and references therein). Hoier and Whitson in [16] developed a model for non-isothermal compositional grading using

Date: March 17, 2020.

2010 Mathematics Subject Classification. 65N30; 65N50; 49S05.

Key words and phrases. Convex splitting, thermodynamically consistent schemes, unbiased schemes, the Peng-Robinson equation of state, compositional variation, gravity effect.

*Corresponding author: Shuyu Sun (shuyu.sun@kaust.edu.sa).

the theory of irreversible processes. Nikpoor et al. applied a nonisothermal model to study compositional variation in a petroleum fluid column [40]. Many other scientists have studied many other factors that lead to the composition of petroleum fluids in subsurface circumstances including: thermal diffusion by Dougherty and Drickamer in 1955 [6], asphaltene precipitation by Riemens et al. in 1988 [48], capillary forces by Lee in 1989 in [27] and Wheaton in 1991 [54], biodegradation by Temeng et al. in 1998 [53], genesis by Smalley and England in 1992 [51], natural convection by Ghorayeb and Firoozabadi in [12], unsteady flux of a water aquifer partly contacting a reservoir by Hoier and Whitson in 2001 [16], reservoir compartmentalization by Elshahawi et al. in 2005 [7], and incomplete hydrocarbon migration by Gibson et al. in 2006 [14]. Enormous research in this area is still active (see [5, 18, 26, 30, 38, 39, 41, 42, 52] and references therein).

All the study reviewed above has been focusing on the prediction of compositional grading features at steady states based on the framework of Gibbs free energy. Kou and Sun in [20] constructed models that can dynamically describe the evolutionary process of compositional grading, and it satisfies the energy dissipation property. The models based on the laws of thermodynamics and multi-component diffusion equations [24, 25, 56] were formulated for laboratory scale (free spaces without solids) and porous media (geophysical scale). And they designed energy-stable numerical methods to solve the proposed models. In the numerical scheme they used a correction term to reformulate the Helmholtz free energy density and a convex-concave splitting of the energy was constructed, which can guarantee the energy decaying property. As long as the correction term is sufficiently big the convex-concave splitting can always work. However, the added term introduces some extra errors and is not theoretically studied to guarantee that the errors are minimized. Secondly, there are usually a large number of species in the hydrocarbon mixture, the proposed numerical methods in literature might be computationally demanding for the big system.

To overcome the two issues above, we will present some numerical schemes for the dynamical models. The proposed methods in this work will introduce physics-preserving terms into the Helmholtz free energy density and energy-decaying numerical and efficient numerical schemes are developed for the models.

The rest of the manuscript is structured as below. In Section 2 and Section 3, we will present the mathematical models for dynamical compositional grading by gravity. The numerical schemes are constructed in Section 4. In Section 5, some numerical experiments are shown to verify the proposed numerical schemes.

2. MATHEMATICAL MODELS FOR COMPOSITIONAL GRADING BY GRAVITY

2.1. Energy functional for compositional grading by gravity. We consider a closed system including a mixture of M species with fixed total mole numbers of each component and temperature being constant. We denote by $n_i(\mathbf{x})$ (n_i for short) the molar density of species i , ($i = 1, \dots, M$) at $\mathbf{x} \in \Omega$, Ω the computational domain. Further we let $\mathbf{n} = (n_1, \dots, n_M)$ and $n = \sum_{i=1}^M n_i$. It is noticed that there has been some research on thermodynamic phase calculation under condition of constant volume, moles and temperature in the literature [10, 11, 17, 19–24, 33, 44, 45, 47]. In this condition the Helmholtz free energy F is naturally adopted. For compositional grading by gravity the total free energy F_{tot} is composed of Helmholtz free energy F and the gravitational potential energy F_g :

$$(2.1) \quad F_{\text{tot}}(\mathbf{n}) = F(\mathbf{n}) + F_g(\mathbf{n})$$

wherein $F(\mathbf{n}) = \int_{\Omega} f(\mathbf{n}) d\mathbf{x}$ and $F_g(\mathbf{n}) = \int_{\Omega} f_g(\mathbf{n}) d\mathbf{x}$. The Helmholtz free energy density f and gravitational potential energy density f_g are respectively expressed as below:

$$(2.2) \quad f_g = \rho g h$$

where g is the gravity acceleration constant, h is the straight distance from the bottom against the direction of gravity acceleration and ρ is mass density of the mixture calculated by

$$(2.3) \quad \rho = \sum_{i=1}^M n_i M_i$$

where M_i is molecular weight of species i . When the Van der Waals or the Peng-Robinson equation of state is applied, the Helmholtz free energy density is expressed by summation of three parts:

$$(2.4) \quad f(\mathbf{n}) = f^{\text{ideal}}(\mathbf{n}) + f^b(\mathbf{n}) + f^a(\mathbf{n}).$$

The details of $f^{\text{ideal}}(\mathbf{n})$, $f^b(\mathbf{n})$ and $f^a(\mathbf{n})$ are given in the appendix. From thermodynamics the definition of chemical potential of species i is given by

$$(2.5) \quad \mu_i(\mathbf{n}) = \left(\frac{\partial f(\mathbf{n})}{\partial n_i} \right)_{T, n_1, \dots, n_{i-1}, n_{i+1}, \dots, n_M}.$$

The thermodynamic pressure can be computed by

$$(2.6) \quad p = \sum_{i=1}^M n_i \mu_i - f,$$

which results in the following relationship

$$(2.7) \quad \nabla p = \sum_{i=1}^M n_i \nabla \mu_i.$$

3. MATHEMATICAL MODELS FOR EVOLUTION OF COMPOSITIONAL GRADING

In this section, we review two types of dynamical models for compositional grading by gravity. In [20] Kou and Sun proposed the following model for dynamically describing the evolution of compositional grading of multicomponent mixture under gravity in free spatial domain and in porous media.

3.1. Dynamical system of compositional grading under gravity. Ignoring the convection, the dynamical process of compositional grading is modeled by the diffusion process in free area

$$(3.8) \quad \frac{\partial n_i}{\partial t} + \nabla \cdot \mathbf{J}_i = 0, \quad i = 1, \dots, M,$$

where \mathbf{J}_i is the diffusion flux of species i given by

$$(3.9) \quad \mathbf{J}_i = -\frac{Dn_i}{RT} \nabla (\mu_i(\mathbf{n}(\mathbf{x}, t)) + M_i gh).$$

We consider a closed system, so we impose the following boundary condition

$$(3.10) \quad \mathbf{J}_i \cdot \boldsymbol{\nu}_{\partial\Omega} = 0, \quad i = 1, \dots, M,$$

where $\boldsymbol{\nu}_{\partial\Omega}$ stands for the normal unit outward vector to the boundary $\partial\Omega$. And the initial conditions are provided as below

$$(3.11) \quad n_i(\mathbf{x}, t = 0) = n_i^{\text{init}}(\mathbf{x}), \quad i = 1, \dots, M.$$

In the porous media the diffusion equations become

$$(3.12) \quad \phi \frac{\partial n_i}{\partial t} + \nabla \cdot \mathbf{J}_i = 0, \quad i = 1, \dots, M.$$

In porous media the diffusion coefficients must be corrected by the porosity ϕ and the tortuosity τ (see [3] and references therein) and therefore the diffusion flux of component i is computed by

$$(3.13) \quad \mathbf{J}_i = -\frac{\phi}{\tau^2} \frac{Dn_i}{RT} \nabla (\mu_i(\mathbf{n}(\mathbf{x}, t)) + M_i gh),$$

which is imposed with the boundary conditions as (3.10) and initial conditions (3.11). Herein we assume that the porous media is incompressible so that the porosity of the rock is time independent.

In [29] Li and Sun presented a model for modeling the development of compositional grading process as below

$$(3.14) \quad \mathcal{M}_i \frac{\partial n_i}{\partial t} + \mu_i(\mathbf{n}(\mathbf{x}, t)) + M_i gh - L_i = 0,$$

$$(3.15) \quad \int_{\Omega} n_i d\mathbf{x} = N_i^t,$$

$$(3.16) \quad n_i(\mathbf{x}, t = 0) = n_i^{\text{init}}(\mathbf{x}),$$

where \mathcal{M}_i is given parameter and L_i is constant function only dependent on time variable. (3.15) is to enforce the mass conservation of the system.

3.2. Energy dissipation property of the dynamical systems. The systems presented above are energy dissipative as described in the following theorems.

Theorem 3.1. (For the proof, see [20].) The three systems (3.8)-(3.11), (3.12)-(3.13) and (3.14)-(3.16) are respectively energy decaying and mass conservativation, in other words,

$$(3.17) \quad \frac{dF_{\text{tot}}}{dt} \leq 0 \text{ and } \frac{d}{dt} \int_{\Omega} n_i d\mathbf{x} = 0.$$

4. NUMERICAL SCHEMES FOR THE COMPOSITIONAL GRADING MODELS

In this section, we will introduce some computationally efficient, energy-stable and easy-to-implement numerical schemes for the compositional grading systems in Section 3. The numerical schemes are based on the property of Helmholtz free energy density. We will consider two types of fluids in terms of the Helmholtz free energy density: the Van der Waals fluids and the Peng-Robinson fluids. The proposed semi-implicit schemes are unconditionally energy stable, which might not be guaranteed by fully explicit and fully implicit temporal discretization schemes [55].

For convenience of analysis, we let $\mathbf{n}^{k+\frac{i}{M}}$ ($i = 1, \dots, M$) be a vector of $(n_1^{k+1}, \dots, n_i^{k+1}, n_{i+1}^k, \dots, n_M^k)$, the j th element of which has the property

$$n_j^{k+\frac{i}{M}} = \begin{cases} n_j^{k+1}, & \text{if } j \leq i, \\ n_j^k, & \text{if } j > i. \end{cases}$$

4.1. Efficient and energy-stable numerical schemes for the dynamical systems of Van der Waals fluids. We present the numerical schemes in this section for the systems (3.8)-(3.11), (3.12)-(3.13) and (3.14)-(3.16) based on Van der Waals fluids.

For the system (3.8)-(3.11) with the Van der Waals model we propose an unconditionally stable scheme as follows:

$$(4.18) \quad \frac{n_i^{k+1} - n_i^k}{\delta t} + \nabla \cdot \mathbf{J}_i^{k+\frac{i}{M}} = 0,$$

$$(4.19) \quad \mathbf{J}_i^{k+\frac{i}{M}} = -\frac{Dn_i^k}{RT} \left(\nabla \mu_i^{\text{convex}}(\mathbf{n}^{k+\frac{i}{M}}) + \nabla \mu_i^{\text{concave}}(\mathbf{n}^{k+\frac{i-1}{M}}) + M_i g \nabla h \right),$$

$$(4.20) \quad \mathbf{J}_i^{k+\frac{i}{M}} \cdot \boldsymbol{\nu}_{\partial\Omega} = 0,$$

$$(4.21) \quad n_i^0(\mathbf{x}) = n_i^{\text{init}}(\mathbf{x}).$$

For the system (3.12)-(3.13) with the Van der Waals model we give the following time-discrete space-continuous scheme:

$$(4.22) \quad \phi \frac{n_i^{k+1} - n_i^k}{\delta t} + \nabla \cdot \mathbf{J}_i^{k+\frac{i}{M}} = 0,$$

$$(4.23) \quad \mathbf{J}_i^{k+\frac{i}{M}} = -\frac{\phi Dn_i^k}{\tau^2 RT} \left(\nabla \mu_i^{\text{convex}}(\mathbf{n}^{k+\frac{i}{M}}) + \nabla \mu_i^{\text{concave}}(\mathbf{n}^{k+\frac{i-1}{M}}) + M_i g \nabla h \right)$$

$$(4.24) \quad \mathbf{J}_i^{k+\frac{i}{M}} \cdot \boldsymbol{\nu}_{\partial\Omega} = 0,$$

$$(4.25) \quad n_i^0(\mathbf{x}) = n_i^{\text{init}}(\mathbf{x}).$$

For the system (3.14)-(3.16) with the Van der Waals model we propose a scheme as below:

$$(4.26) \quad \frac{n_i^{k+1} - n_i^k}{\delta t} + \mu_i^{\text{convex}}(\mathbf{n}^{k+\frac{i}{M}}) + \mu_i^{\text{concave}}(\mathbf{n}^{k+\frac{i-1}{M}}) + M_i gh - L_i^{k+1} = 0,$$

$$(4.27) \quad \int_{\Omega} n_i^{k+1} d\mathbf{x} = N_i^t,$$

$$(4.28) \quad n_i^0(\mathbf{x}) = n_i^{\text{init}}(\mathbf{x}).$$

In the above systems for Van der Waals fluids, $\mu_i^{\text{convex}}(\mathbf{n}^{k+\frac{i}{M}})$ and $\mu_i^{\text{concave}}(\mathbf{n}^{k+\frac{i-1}{M}})$ are respectively given by

$$(4.29) \quad \mu_i^{\text{convex}}(\mathbf{n}^{k+\frac{i}{M}}) = \left. \frac{\partial f^{\text{ideal}}(\mathbf{n})}{\partial n_i} \right|_{\mathbf{n}=\mathbf{n}^{k+\frac{i}{M}}} + \left. \frac{\partial f^{\text{b}}(\mathbf{n})}{\partial n_i} \right|_{\mathbf{n}=\mathbf{n}^{k+\frac{i}{M}}}$$

$$(4.30) \quad \mu_i^{\text{concave}}(\mathbf{n}^{k+\frac{i-1}{M}}) = \left. \frac{\partial f^{\text{a}}(\mathbf{n})}{\partial n_i} \right|_{\mathbf{n}=\mathbf{n}^{k+\frac{i-1}{M}}}$$

Lemma 4.1. For the Van der Waals fluids, $\frac{\partial f^{\text{ideal}}(\mathbf{n})}{\partial n_i}$ and $\frac{\partial f^{\text{b}}(\mathbf{n})}{\partial n_i}$ are both convex with respect to n_i , namely,

$$(4.31) \quad \frac{\partial^2 f^{\text{ideal}}(\mathbf{n})}{\partial n_i^2} \geq 0 \text{ and } \frac{\partial^2 f^{\text{b}}(\mathbf{n})}{\partial n_i^2} \geq 0,$$

while $\frac{\partial f^{\text{a}}(\mathbf{n})}{\partial n_i}$ is a concave function of n_i , i.e.,

$$(4.32) \quad \frac{\partial^2 f^{\text{a}}(\mathbf{n})}{\partial n_i^2} \leq 0.$$

Proof. We recall that $f^{\text{ideal}} = RT \sum_{i=1}^M n_i (\ln n_i - 1)$, $f^{\text{b}} = -RTn \ln(1 - bn)$ and $f^{\text{a}} = -an^2$. We have

$$\frac{\partial f^{\text{ideal}}}{\partial n_i} = RT \ln n_i, \quad \frac{\partial^2 f^{\text{ideal}}}{\partial n_i^2} = RT \frac{1}{n_i} > 0.$$

Similarly, we have

$$\frac{\partial^2 f^{\text{b}}}{\partial n_i^2} = RT \left(\frac{2b_i}{1 - bn} + \frac{b_i^2 n}{(1 - bn)^2} \right).$$

According to the Van der Waals theory $(1 - bn) > 0$, $b_i > 0$ and $n > 0$, we have $\frac{\partial^2 f^{\text{b}}}{\partial n_i^2} > 0$. Finally, first order partial derivative of f^{a} with n_i gives

$$\frac{\partial f^{\text{a}}}{\partial n_i} = -2 \sum_{j=1}^M a_{ij} n_j.$$

And hence second order partial derivative of f^{a} with n_i is

$$\frac{\partial^2 f^{\text{a}}}{\partial n_i^2} = -2a_{ii} < 0.$$

□

Theorem 4.2. The semi-discrete schemes (4.18) - (4.21), (4.22)- (4.25) and (4.26)- (4.28) are respectively energy decreasing for each i , that is, for any time step size $\delta t > 0$ the total free energy satisfies

$$(4.33) \quad F^{\text{tot}}(\mathbf{n}^{k+\frac{i}{M}}) \leq F^{\text{tot}}(\mathbf{n}^{k+\frac{i-1}{M}}), \quad i = 1, \dots, M.$$

Proof. From Lemma 4.1, we conclude that $f^{\text{ideal}}(\mathbf{n}^{k+\frac{i}{M}})$ and $f^{\text{ideal}}(\mathbf{n}^{k+\frac{i}{M}})$ are convex functions of n_i^{k+1} . We have

$$(4.34) \quad \left(\frac{\partial f^{\text{ideal}}}{\partial n_i} \Big|_{\mathbf{n}=\mathbf{n}^{k+\frac{i}{M}}}, n_i^{k+1} - n_i^k \right) \geq f^{\text{ideal}}(\mathbf{n}^{k+\frac{i}{M}}) - f^{\text{ideal}}(\mathbf{n}^{k+\frac{i-1}{M}}),$$

$$(4.35) \quad \left(\frac{\partial f^{\text{b}}}{\partial n_i} \Big|_{\mathbf{n}=\mathbf{n}^{k+\frac{i}{M}}}, n_i^{k+1} - n_i^k \right) \geq f^{\text{b}}(\mathbf{n}^{k+\frac{i}{M}}) - f^{\text{b}}(\mathbf{n}^{k+\frac{i-1}{M}}).$$

$f^{\text{a}}(\mathbf{n}^{k+\frac{i}{M}})$ is concave with respect to n_i^{k+1} , and therefore

$$(4.36) \quad \left(\frac{\partial f^{\text{a}}}{\partial n_i} \Big|_{\mathbf{n}=\mathbf{n}^{k+\frac{i-1}{M}}}, n_i^{k+1} - n_i^k \right) \geq f^{\text{a}}(\mathbf{n}^{k+\frac{i}{M}}) - f^{\text{a}}(\mathbf{n}^{k+\frac{i-1}{M}}).$$

(4.34), (4.35) and (4.36) are equivalently written as

$$(4.37) \quad \left(\mu_i^{\text{ideal}} \left(\mathbf{n}^{k+\frac{i}{M}} \right), n_i^{k+1} - n_i^k \right) \geq f^{\text{ideal}}(\mathbf{n}^{k+\frac{i}{M}}) - f^{\text{ideal}}(\mathbf{n}^{k+\frac{i-1}{M}}),$$

$$(4.38) \quad \left(\mu_i^{\text{b}} \left(\mathbf{n}^{k+\frac{i}{M}} \right), n_i^{k+1} - n_i^k \right) \geq f^{\text{b}}(\mathbf{n}^{k+\frac{i}{M}}) - f^{\text{b}}(\mathbf{n}^{k+\frac{i-1}{M}}),$$

and

$$(4.39) \quad \left(\mu_i^{\text{a}} \left(\mathbf{n}^{k+\frac{i-1}{M}} \right), n_i^{k+1} - n_i^k \right) \geq f^{\text{a}}(\mathbf{n}^{k+\frac{i}{M}}) - f^{\text{a}}(\mathbf{n}^{k+\frac{i-1}{M}}).$$

For the gravitational potential energy density

$$(4.40) \quad f_g \left(\mathbf{n}^{k+\frac{i}{M}} \right) - f_g \left(\mathbf{n}^{k+\frac{i-1}{M}} \right) = (n_i^{k+1} - n_i^k) M_i g h.$$

Multiplying (4.18) by $\delta t \left(\mu_i^{\text{ideal}} \left(\mathbf{n}^{k+\frac{i}{M}} \right) + \mu_i^{\text{b}} \left(\mathbf{n}^{k+\frac{i}{M}} \right) + \mu_i^{\text{a}} \left(\mathbf{n}^{k+\frac{i-1}{M}} \right) + M_i g h \right)$ and taking integration over Ω we have

$$(4.41) \quad \begin{aligned} & F^{\text{tot}}(\mathbf{n}^{k+\frac{i}{M}}) - F^{\text{tot}}(\mathbf{n}^{k+\frac{i-1}{M}}) \\ &= F^{\text{ideal}}(\mathbf{n}^{k+\frac{i}{M}}) - F^{\text{ideal}}(\mathbf{n}^{k+\frac{i-1}{M}}) + \\ & \quad F^{\text{b}}(\mathbf{n}^{k+\frac{i}{M}}) - F^{\text{b}}(\mathbf{n}^{k+\frac{i-1}{M}}) + \\ & \quad F^{\text{a}}(\mathbf{n}^{k+\frac{i}{M}}) - F^{\text{a}}(\mathbf{n}^{k+\frac{i-1}{M}}) + \\ & \quad F_g \left(\mathbf{n}^{k+\frac{i}{M}} \right) - F_g \left(\mathbf{n}^{k+\frac{i-1}{M}} \right) \\ (4.42) \quad & \leq \left(\mu_i^{\text{ideal}} \left(\mathbf{n}^{k+\frac{i}{M}} \right), n_i^{k+1} - n_i^k \right) + \\ & \quad \left(\mu_i^{\text{b}} \left(\mathbf{n}^{k+\frac{i}{M}} \right), n_i^{k+1} - n_i^k \right) + \\ & \quad \left(\mu_i^{\text{a}} \left(\mathbf{n}^{k+\frac{i-1}{M}} \right), n_i^{k+1} - n_i^k \right) + \\ & \quad (M_i g h, n_i^{k+1} - n_i^k) \\ &= -\delta t \left(\mu_i^{\text{ideal}} \left(\mathbf{n}^{k+\frac{i}{M}} \right) + \mu_i^{\text{b}} \left(\mathbf{n}^{k+\frac{i}{M}} \right) + \mu_i^{\text{a}} \left(\mathbf{n}^{k+\frac{i-1}{M}} \right) + M_i g h, \nabla \cdot \mathbf{J}_i^{k+\frac{i}{M}} \right) \\ &= \delta t \int_{\Omega} \nabla \left(\mu_i^{\text{ideal}} \left(\mathbf{n}^{k+\frac{i}{M}} \right) + \mu_i^{\text{b}} \left(\mathbf{n}^{k+\frac{i}{M}} \right) + \mu_i^{\text{a}} \left(\mathbf{n}^{k+\frac{i-1}{M}} \right) + M_i g h \right) \cdot \mathbf{J}_i^{k+\frac{i}{M}} d\mathbf{x} \\ &= -\delta t \int_{\Omega} \frac{Dn_i^k}{RT} \left| \nabla \left(\mu_i^{\text{ideal}} \left(\mathbf{n}^{k+\frac{i}{M}} \right) + \mu_i^{\text{b}} \left(\mathbf{n}^{k+\frac{i}{M}} \right) + \mu_i^{\text{a}} \left(\mathbf{n}^{k+\frac{i-1}{M}} \right) + M_i g h \right) \right|^2 \\ & \leq 0. \end{aligned}$$

And hence

$$(4.43) \quad F^{\text{tot}}(\mathbf{n}^{k+\frac{i}{M}}) \leq F^{\text{tot}}(\mathbf{n}^{k+\frac{i-1}{M}}).$$

It is straightforward to see that

$$(4.44) \quad F^{\text{tot}}(\mathbf{n}^{k+1}) = F^{\text{tot}}(\mathbf{n}^{k+\frac{M}{M}}) \leq F^{\text{tot}}(\mathbf{n}^{k+\frac{M-1}{M}}) \leq \dots \leq F^{\text{tot}}(\mathbf{n}^{k+\frac{1}{M}}) \leq F^{\text{tot}}(\mathbf{n}^{k+\frac{0}{M}}) = F^{\text{tot}}(\mathbf{n}^k).$$

In a similar way, we can prove that (4.43) and (4.44) hold true for systems (3.12)-(3.13) and (3.14)-(3.16). \square

4.2. Efficient and energy-stable numerical schemes for the dynamical systems of the Peng-Robinson fluids. For the Peng-Robinson fluids, f^{ideal} and f^{b} are the same as for Van der Waals fluids, but f^{a} is different that we take into account in this section.

Denote \tilde{b} by $\sum_{j=1}^M b_j n_j$, \tilde{a}_i by $\sum_{j=1}^M a_{ij} n_j$ and \tilde{a} by $\sum_{j=1}^M \sum_{k=1}^M a_{jk} n_k n_j$. Let $\tilde{f}(\mathbf{n}) = f^{\text{ideal}}(\mathbf{n}) + f^{\text{b}}(\mathbf{n}) + f^{\text{a}}(\mathbf{n}) + \frac{1}{2} K \hat{a} n^2 - \frac{1}{2} K \hat{a} n^2$, where $f^{\text{ideal}}(\mathbf{n}) = RT \sum_{i=1}^M n_i (\ln n_i - 1)$, $f^{\text{b}}(\mathbf{n}) = -nRT \ln(1 - bn)$, $f^{\text{a}}(\mathbf{n}) =$

$\frac{\tilde{a}}{2\sqrt{2}\tilde{b}} \ln \left(\frac{1+(1-\sqrt{2})\tilde{b}}{1+(1+\sqrt{2})\tilde{b}} \right)$, $\hat{a} = \sum_{i,j=1}^M \sqrt{a_i a_j} x_i x_j$, and K is a non-negative real constant and its computation will be given in subsequent sections.

Remark 4.1. Here the term $\frac{1}{2}K\hat{a}n^2$ is similar to $-an^2$ which stands for the energy density f^a as in the Van der Waals fluids but here $k_{ij} = 0$ in the mixing rule. The added term to Peng-Robinson fluids is physics-preserving and the Helmholtz free energy density is not changed. More advantageously, $\hat{A} = (\hat{a}_{ij})_{M \times M} = (\sqrt{a_i a_j})_{M \times M}$ is positive semidefinite and $a_i = \hat{a}_{ii} > 0$, which plays an important role in the numerical schemes.

Rewrite $\tilde{f}(\mathbf{n})$ as

$$\tilde{f}(\mathbf{n}) = \left(f^{\text{ideal}}(\mathbf{n}) + f^b(\mathbf{n}) + \frac{1}{2}K\hat{a}n^2 \right) + \left(f^a(\mathbf{n}) - \frac{1}{2}K\hat{a}n^2 \right).$$

We give the following lemma.

Lemma 4.3. If $K \geq 0$, then $f^{\text{conv}} = f^{\text{ideal}}(\mathbf{n}) + f^b + \frac{1}{2}K\hat{a}n^2$ is a convex function of n_i , otherwise stated, $\frac{\partial^2 f^{\text{conv}}}{\partial n_i^2} > 0$.

Proof. It is easy to prove.

$$\frac{\partial^2 f^{\text{conv}}}{\partial n_i^2} = \frac{\partial^2 f^{\text{ideal}}}{\partial n_i^2} + \frac{\partial^2 f^b}{\partial n_i^2} + K\hat{a}_{ii},$$

from Lemma (4.1), $\frac{\partial^2 f^{\text{ideal}}}{\partial n_i^2} + \frac{\partial^2 f^b}{\partial n_i^2} > 0$ and $K \geq 0$, so $\frac{\partial^2 f^{\text{conv}}}{\partial n_i^2} > 0$. \square

For the second part of \tilde{f}_0 we have the following lemma.

Lemma 4.4. If we take

$$(4.45) \quad K \geq \max \left\{ -\frac{b_i \left(2\tilde{a}_i \tilde{b} - b_i \tilde{a} \right)}{\sqrt{2} a_i \tilde{b}^3} \ln \left(\frac{1 + (1 - \sqrt{2}) \tilde{b}}{1 + (1 + \sqrt{2}) \tilde{b}} \right) - \frac{2b_i \left(2\tilde{b} \tilde{a}_i \left(1 + 2\tilde{b} - \tilde{b}^2 \right) - b_i \tilde{a} \left(1 + 3\tilde{b} - 2\tilde{b}^2 \right) \right)}{a_i \tilde{b}^2 \left(1 + (1 - \sqrt{2}) \tilde{b} \right)^2 \left(1 + (1 + \sqrt{2}) \tilde{b} \right)^2}, 0 \right\},$$

then $\tilde{f}^a(\mathbf{n}) = f^a(\mathbf{n}) - \frac{1}{2}K\hat{a}n^2$ is a concave function of n_i or $\frac{\partial^2 \tilde{f}^a(\mathbf{n})}{\partial n_i^2} < 0$.

The proof is straightforward.

Based on the above analysis, the total Helmholtz free energy density of the Peng-Robinson fluids is written as summation of two parts:

$$(4.46) \quad \tilde{f}(\mathbf{n}) = \left(f^{\text{ideal}}(\mathbf{n}) + f^b(\mathbf{n}) + \frac{1}{2}K\hat{a}n^2 \right) + \left(f^a(\mathbf{n}) - \frac{1}{2}K\hat{a}n^2 \right),$$

where K satisfies (4.45).

We propose the following numerical schemes in this section for the systems (3.8)-(3.11), (3.12)-(3.13) and (3.14)-(3.16) for Peng-Robinson fluids.

For the system (3.8)-(3.11) with the Peng-Robinson fluids we give the time discretization scheme below:

$$(4.47) \quad \frac{n_i^{k+1} - n_i^k}{\delta t} + \nabla \cdot \mathbf{J}_i^{k+\frac{i}{M}} = 0,$$

$$(4.48) \quad \mathbf{J}_i^{k+\frac{i}{M}} = -\frac{Dn_i^k}{RT} \left(\nabla \tilde{\mu}_i^{\text{convex}}(\mathbf{n}^{k+\frac{i}{M}}) + \nabla \tilde{\mu}_i^{\text{concave}}(\mathbf{n}^{k+\frac{i-1}{M}}) + M_i g \nabla h \right),$$

$$(4.49) \quad \mathbf{J}_i^{k+\frac{i}{M}} \cdot \boldsymbol{\nu}_{\partial\Omega} = 0,$$

$$(4.50) \quad n_i^0(\mathbf{x}) = n_i^{\text{init}}, \quad i = 1, \dots, M.$$

For the system (3.12)-(3.13) with the Peng-Robinson fluids we give the following time-discrete space-continuous scheme:

$$(4.51) \quad \phi \frac{n_i^{k+1} - n_i^k}{\delta t} + \nabla \cdot \tilde{\mathbf{J}}_i^{k+\frac{i}{M}} = 0,$$

$$(4.52) \quad \tilde{\mathbf{J}}_i^{k+\frac{i}{M}} = -\frac{\phi}{\tau^2} \frac{Dn_i^k}{RT} \left(\nabla \tilde{\mu}_i^{\text{convex}}(\mathbf{n}^{k+\frac{i}{M}}) + \nabla \tilde{\mu}_i^{\text{concave}}(\mathbf{n}^{k+\frac{i-1}{M}}) + M_i g \nabla h \right),$$

$$(4.53) \quad \tilde{\mathbf{J}}_i^{k+\frac{i}{M}} \cdot \boldsymbol{\nu}_{\partial\Omega} = 0,$$

$$(4.54) \quad n_i^0(\mathbf{x}) = n_i^{\text{init}}.$$

For the system (3.14)-(3.16) with the Peng-Robinson fluids we propose a scheme as below:

$$(4.55) \quad \frac{n_i^{k+1} - n_i^k}{\delta t} + \tilde{\mu}_i^{\text{convex}}(\mathbf{n}^{k+\frac{i}{M}}) + \tilde{\mu}_i^{\text{concave}}(\mathbf{n}^{k+\frac{i-1}{M}}) + M_i g \nabla h - L_i^{k+1} = 0,$$

$$(4.56) \quad \int_{\Omega} n_i^{k+1} d\mathbf{x} = N_i^t,$$

$$(4.57) \quad n_i(\mathbf{x}, t=0) = n_i^{\text{init}}.$$

In the above systems for the Peng-Robinson fluids, $\tilde{\mu}_i^{\text{convex}}(\mathbf{n}^{k+\frac{i}{M}})$ and $\tilde{\mu}_i^{\text{concave}}(\mathbf{n}^{k+\frac{i-1}{M}})$ are respectively given by

$$(4.58) \quad \tilde{\mu}_i^{\text{convex}}(\mathbf{n}^{k+\frac{i}{M}}) = \frac{\partial f^{\text{ideal}}(\mathbf{n})}{\partial n_i} \Big|_{\mathbf{n}=\mathbf{n}^{k+\frac{i}{M}}} + \frac{\partial f^{\text{b}}(\mathbf{n})}{\partial n_i} \Big|_{\mathbf{n}=\mathbf{n}^{k+\frac{i}{M}}} + K \sum_{j=1}^M a_{ij} n_j \Big|_{\mathbf{n}=\mathbf{n}^{k+\frac{i}{M}}},$$

$$(4.59) \quad \tilde{\mu}_i^{\text{concave}}(\mathbf{n}^{k+\frac{i-1}{M}}) = \frac{\partial f^{\text{a}}(\mathbf{n})}{\partial n_i} \Big|_{\mathbf{n}=\mathbf{n}^{k+\frac{i-1}{M}}} - K \sum_{j=1}^M a_{ij} n_j \Big|_{\mathbf{n}=\mathbf{n}^{k+\frac{i-1}{M}}},$$

where K satisfies (4.45).

Theorem 4.5. The semi-discrete schemes (4.47) - (4.50), (4.51)- (4.54) and (4.55)- (4.57) are respectively energy decreasing for each i , otherwise stated, for any large time step size $\delta t > 0$ the total free energy satisfies

$$(4.60) \quad F^{\text{tot}}(\mathbf{n}^{k+\frac{i}{M}}) \leq F^{\text{tot}}(\mathbf{n}^{k+\frac{i-1}{M}}), \quad i = 1, \dots, M.$$

Proof. It can be proved in a similar way as for the Van der Waals fluids. \square

4.3. Spatial discretization by Raviart-Thomas mixed finite element methods. The Raviart-Thomas mixed finite element (RT-MFEM) [24, 25] is widely adopted in discretizing partial differential equations of flow problems especially in reservoir simulation for its advantages of local mass conservation and accurate approximation of both scalar and vector functions simultaneously even with lowest-order element [1, 2, 4]. The RT-MFEM is suitable for the time-discrete space-continuous systems described in the above section.

For simplicity the two-dimensional ($d = 2$) computational domain Ω is divided into triangular meshes. Let \mathcal{T}_h represent the partition of Ω . Denote Γ_h by the interior edges of \mathcal{T}_h . Denote ν_e by the unit normal vector for each edge $e \in \Gamma_h$; which is accordant with the outward unit normal vector on the boundary of the domain. Define

$$(4.61) \quad \mathbf{V} \equiv H(\Omega; \text{div}) \equiv \left\{ \mathbf{v} \in (L^2(\Omega))^d : \nabla \cdot \mathbf{v} \in L^2(\Omega) \right\},$$

$$(4.62) \quad W \equiv L^2(\Omega).$$

Denote (\cdot, \cdot) and $\langle \cdot, \cdot \rangle_{\Gamma}$ by the inner product in $(L^2(\Omega))^d$ or $L^2(\Omega)$ and $L^2(\Gamma)$, respectively. Because the Van der Waals and the Peng-Robinson models have the same time-discrete form, for convenience, the space-discretization will be described in one single formula based on (4.47)- (4.50), when the Van der Waals model is considered $K \equiv 0$. We note that (4.55)- (4.57) is not needed to use MFEM for spatial discretization.

The first step is to formulate a weak formulation of (4.47)- (4.50): to seek $n_i^{k+\frac{i}{M}} \in W$ and $\tilde{\mathbf{J}}_i^{k+\frac{i}{M}} \in V$ such that

$$(4.63) \quad \left(\phi \frac{n_i^{k+1} - n_i^k}{\delta t}, w \right) + \left(\nabla \cdot \tilde{\mathbf{J}}_i^{k+\frac{i}{M}}, w \right) = 0, \forall w \in W,$$

$$(4.64) \quad \left(\frac{RT}{Dn_i^k} \tilde{\mathbf{J}}_i^{k+\frac{i}{M}}, \mathbf{v} \right) = \left(\nabla \tilde{\mu}_i(\mathbf{n}^{k+\frac{i}{M}}) + M_i g \nabla h, \nabla \cdot \mathbf{v} \right), \forall \mathbf{v} \in V,$$

$$(4.65) \quad (n_i^0(\mathbf{x}), w) = (n_i^{\text{init}}, w), \forall w \in W,$$

where $\tilde{\mu}_i(\mathbf{n}^{k+\frac{i}{M}}) = \tilde{\mu}_i^{\text{convex}}(\mathbf{n}^{k+\frac{i}{M}}) + \tilde{\mu}_i^{\text{concave}}(\mathbf{n}^{k+\frac{i}{M}})$.

The Raviart-Thomas space of r -th order ($r \geq 0$), RT_r , of the partition \mathcal{T}_h is applied to approximate the subspace $\mathbf{V}_r(\mathcal{T}_h) \times W_r(\mathcal{T}_h)$ of $\mathbf{V} \times W$. For $d = 2$, it is defined as

$$(4.66) \quad \mathbf{V}_r(\mathcal{T}_h) = \{ \mathbf{v} \in H(\Omega; \text{div}) : \mathbf{v}|_E \in \mathbf{Q}_{r+1,r}(\mathbb{E}) \times \mathbf{Q}_{r,r+1}(\mathbb{E}), \mathbb{E} \in \mathcal{T}_h \},$$

$$(4.67) \quad W_r(\mathcal{T}_h) = \{ w \in L^2(\Omega) : w|_E \in Q_{r,r+1}(E), E \in \mathcal{T}_h \},$$

where $Q_{m,n}(E)$ is the space of polynomials of degree less than or equal to $m(n)$ in the first (or second) variable restricted to E . Finally the RT mixed finite element approximation to the system of (4.47)- (4.50)

reads to seek $n_{h,i}^{k+1} \in W_r(\mathcal{T}_h)$ and $\tilde{\mathbf{J}}_{h,i}^{k+\frac{i}{M}} \in \mathbf{V}_r(\mathcal{T}_h)$ such that

$$(4.68) \quad \left(\frac{n_{h,i}^{k+1} - n_{h,i}^k}{\delta t}, w \right) + \left(\nabla \cdot \tilde{\mathbf{J}}_{h,i}^{k+\frac{i}{M}}, w \right) = 0, \forall w \in W_r(\mathcal{T}_h),$$

$$(4.69) \quad \left(\frac{RT}{Dn_{h,i}^k} \tilde{\mathbf{J}}_{h,i}^{k+\frac{i}{M}}, \mathbf{v} \right) = \left(\nabla \tilde{\mu}_i(\mathbf{n}_h^{k+\frac{i}{M}}) + M_i g \nabla h, \nabla \cdot \mathbf{v} \right), \forall \mathbf{v} \in \mathbf{V}_r(\mathcal{T}_h),$$

$$(4.70) \quad (n_{h,i}^0(\mathbf{x}), w) = (n_{h,i}^{\text{init}}, w), \forall w \in W_r(\mathcal{T}_h),$$

where $\tilde{\mu}_i(\mathbf{n}_h^{k+\frac{i}{M}}) = \tilde{\mu}_i^{\text{convex}}(\mathbf{n}_h^{k+\frac{i}{M}}) + \tilde{\mu}_i^{\text{concave}}(\mathbf{n}_h^{k+\frac{i}{M}})$.

Similarly we have the RT-MFEM discretization for system of (4.51)- (4.54)

$$(4.71) \quad \left(\phi_h \frac{n_{h,i}^{k+1} - n_{h,i}^k}{\delta t}, w \right) + \left(\nabla \cdot \tilde{\mathbf{J}}_{h,i}^{k+\frac{i}{M}}, w \right) = 0, \forall w \in W_r(\mathcal{T}_h),$$

$$(4.72) \quad \left(\frac{\tau_h^2}{\phi_h} \frac{RT}{Dn_{h,i}^k} \tilde{\mathbf{J}}_{h,i}^{k+\frac{i}{M}}, \mathbf{v} \right) = \left(\nabla \tilde{\mu}_i(\mathbf{n}_h^{k+\frac{i}{M}}) + M_i g \nabla h, \nabla \cdot \mathbf{v} \right), \forall \mathbf{v} \in \mathbf{V}_r(\mathcal{T}_h),$$

$$(4.73) \quad (n_{h,i}^0(\mathbf{x}), w) = (n_{h,i}^{\text{init}}, w), \forall w \in W_r(\mathcal{T}_h),$$

where $\tilde{\mu}_i(\mathbf{n}_h^{k+\frac{i}{M}}) = \tilde{\mu}_i^{\text{convex}}(\mathbf{n}_h^{k+\frac{i}{M}}) + \tilde{\mu}_i^{\text{concave}}(\mathbf{n}_h^{k+\frac{i}{M}})$.

Theorem 4.6. The fully discrete systems of (4.68)- (4.70) and (4.71)- (4.73) are energy decaying saying that for any large time step size $\delta t > 0$

$$(4.74) \quad F^{\text{tot}}(\mathbf{n}_h^{k+\frac{i}{M}}) \leq F^{\text{tot}}(\mathbf{n}_h^{k+\frac{i-1}{M}}), \quad i = 1, \dots, M.$$

Since the proof is straightforward we ignore it here.

5. NUMERICAL EXAMPLES

In this section, we conduct some numerical experiments to verify the property of our proposed numerical schemes for multicomponent systems. Since in this work we majorly analyze the effect of gravity on the molar concentration along the vertical direction, the composition variation on lateral direction is ignored. Moreover, without loss of generality, all the numerical results are shown for the system of (3.12) and (3.13). All the relevant data for the species used in the numerical examples are tabulated in Tables 1. The porosity is homogeneously distributed as 0.25 for all examples below. The gravitational acceleration constant is taken

as $g = 9.81 \text{ m} \cdot \text{s}^{-2}$. The homogeneous Neumann boundary conditions for diffusion flux are enforced for all examples. RT_0 finite element is utilized for the spatial discretization for all experiments.

To simulate a two-phase case, we must specify some proper initial conditions, which can be done by stability analysis. We adopt the algorithm proposed in [46] to set the initial conditions for two-phase systems.

TABLE 1. Media property parameters and other relevant data

component name	symbol	$T_c(\text{K})$	$P_c(\text{MPa})$	$T_b(\text{K})$
methane	C ₁	190.58	4.604	111.63
ethane	C ₂	305.42	4.88	184.55
propane	C ₃	369.82	4.25	231.05
normal pentane	nC ₅	469.7	3.369	309.22
heptane	C ₇	540.1	2.734	371.57
n-decane	nC ₁₀	617.7	2.099	447.3
nitrogen	N ₂	126.2	3.392	77.5
carbon dioxide	CO ₂	304.4	7.398	194.8

Example 5.1. In this experiment, we consider an ideal gas mixture of nitrogen and carbon dioxide. For ideal gas mixture at equilibrium, an analytical solution can be obtained. The numerical results are validated by the analytic solution. In [20] the authors derived the following analytic solution of composition variation problem for ideal fluids at equilibrium:

$$(5.75) \quad n_i = n_{i,0} e^{-\frac{M_i g z}{RT}},$$

where $n_{i,0}$ is the molar concentration of species i at reference level. In addition, we can calculate the mole fraction x_i of species i in the mixture

$$(5.76) \quad x_i := \frac{n_i}{\sum_{j=1}^M n_j} = \frac{n_{i,0} e^{-\frac{M_i g z}{RT}}}{\sum_{j=1}^M n_{j,0} e^{-\frac{M_j g z}{RT}}}.$$

The temperature is set as $T = 320 \text{ K}$. The computational domain is $[-500\text{m}, 0]$ which is uniformly cut into 500 elements. Initially the molar densities of both nitrogen and methane are homogeneously set as 20 mol/m^3 in the the whole domain. The numerical results of molar density using our proposed numerical scheme is demonstrated in Figure 1. With time marching the molar densities of these two species are approaching to a equilibrium state which is exactly given by Eq. (5.75). At $t = 0.05$ seconds, molar density curve of the simulated results almost fully coincide with the analytical solution. Accordingly, we compute the mole fractions of each species at different time steps, which is shown in Figure 2. From the results in Figures 1 and 2, we can observe that the light component (methane) is "floating" upwards whereas the heavy one is "falling" downwards as time marches. This verifies the gravity effect on the composition variation. The

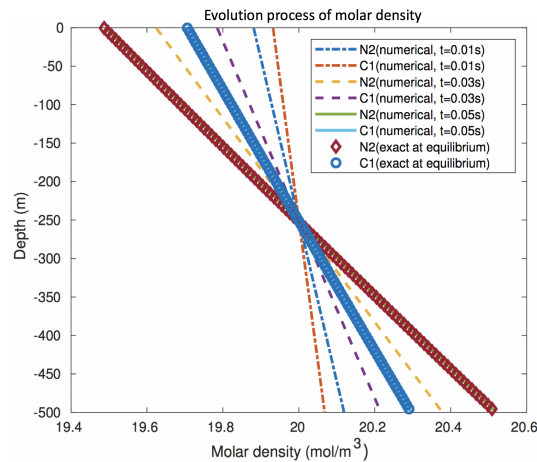


FIGURE 1. Evolution process of molar density

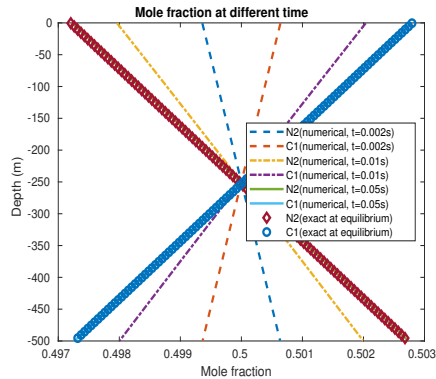


FIGURE 2. Mole fractions at different time

total energy for each time step is displayed in Figure 3. To verify the energy decaying property in species wise we show the energy evolution processes in fractional time step in Figure 3 in blue dash line while the red line is showing the dissipative process at every full time step. In both view of points we can see the the total energy is always decreasing with time.

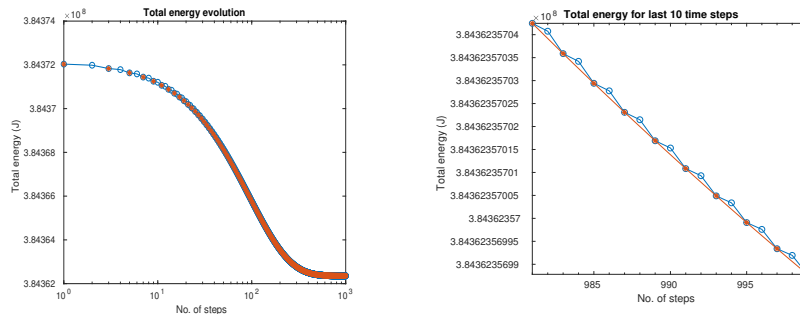


FIGURE 3. Left: Total energy at different time steps; right: zoom-in of total energy at last ten time steps.

Example 5.2. In this example, we illustrate an experiment of phase behavior for a system at near-critical conditions. Carbon hydrocarbon is widely studied for both reservoir engineering and environmental protection, and therefore it is chosen to be as the component at its critical temperature $T = 304.2K$. The computational domain is $[0, 2000m]$ along the vertical direction. The domain is uniformly divided into 400 subintervals. The time step size is taken as $dt = 40$ seconds, for sake of accuracy, though the scheme is unconditionally stable. Initially the molar density is given as the density at critical conditions, i.e., $10640.9 \text{ mol}/m^3$. The molar density evolutionary process is indicated in Figure 4 and the energy changing with time is shown in Figure 5. The results show that there is a significant changing of molar density from the bottom to the top, which results from the influence of gravitational force. The system approaches to an equilibrium state after 250 time steps running, which is rigorously verified by the evolutionary process of total energy in Figure 5.

Example 5.3. In this example, we simulate a more realistic mixture of six hydrocarbon species including both light components and heavy components: methane (C1), ethane (C2), propane (C3), n-pentane (nC5), heptane (C7) and decane (nC10). Temperature keeps $T = 378.2 K$ during the simulation. The domain size

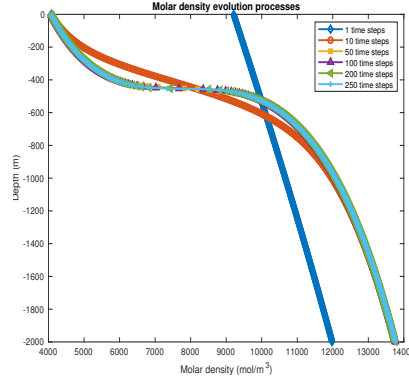


FIGURE 4. Molar density at different time.

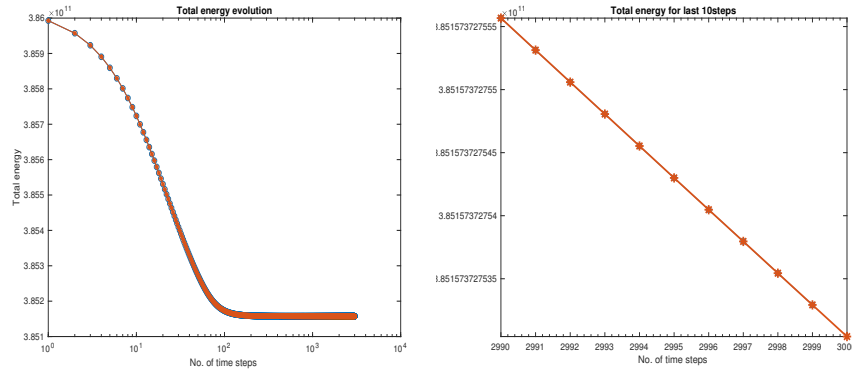


FIGURE 5. Left: Total energy at different time steps; right: zoom-in of total energy at last ten time steps.

is 100 meters and is uniformly split into 100 small intervals. Time step size is taken as $\delta t = 100$ seconds. The molar densities of all species are uniformly set as $500 \text{ mol}/\text{m}^3$ in whole domain.

To verify the unbiased property of the proposed algorithm, we implement this example in random order of the species at the same conditions. Totally there are 720 different sequences of species order. Herein we show the results for six groups of random orders consisting of: (C7, C2, nC10, C1, C3, nC5) in Figures 6 – 8, (C2, C7, C1, C3, nC5, nC10) in Figures 9 – 11, (nC5, C3, nC10, C7, C1, C2) in Figures 12 – 14, (nC10, C2, C1, C7, nC5, C3) in Figures 15 – 17, (nC10, C2, C1, C7, nC5, C3) in Figures 18 – 20, and (nC5, nC10, C7, C1, C2, C3) in Figures 21 – 23.

The molar densities at different time are illustrated in Figures 6, 9, 12, 15, 18, and 21 for the six groups of orders. Initially the molar densities of all species are the same. From these results we observe that as time marches, increasingly more light components assemble at top of the subsurface while more heavy species go to bottom parts of the domain. At convergence there is an apparent interface that divides the fluids into two phases.

Figures 7, 10, 13, 16, 19, and 22 show the mole fractions for the six groups at different time. The results of mole fractions further indicate that the light species flow to the top parts the domain while the dense components sediment to the bottom of the domain due to the effect of gravity.

Figures 8, 11, 14, 17, 20, and 23 show the convergence process of total energy with time for the six groups of different orders. We still compute the total energy in species-wise at each time step in blue while the total energy in each full time step is shown in red. These results verify that the proposed schemes are dissipative in species wise and obviously the total energy is decreasing with time.

From these results in six different groups of order, we have the same molar density distribution (as well as the same mole fraction distribution) at each time step. The total energy is converging to the same value for

all these six different groups. And therefore, we can conclude that the proposed scheme is unbiased in order the species and is more robust.

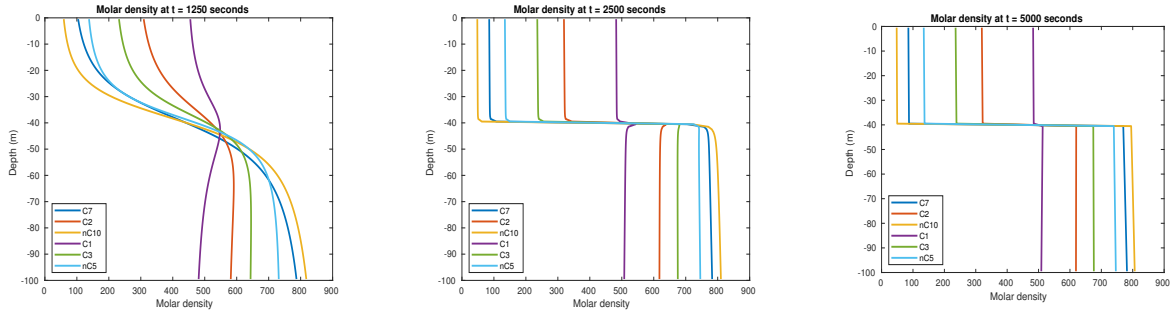


FIGURE 6. Molar density at different time.

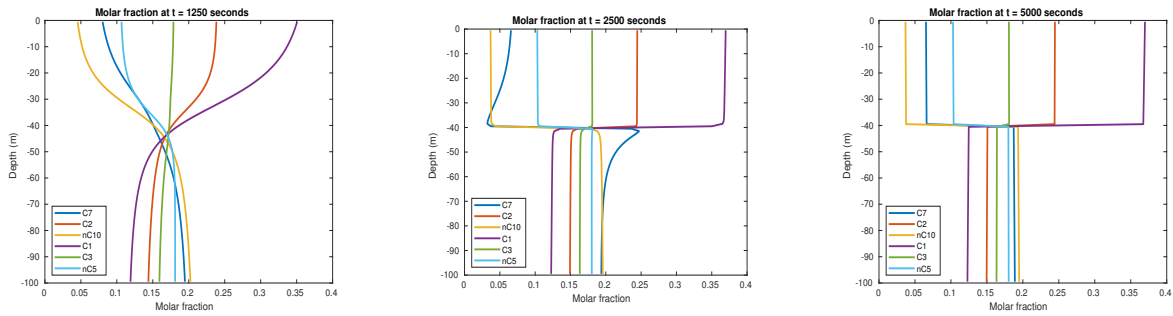


FIGURE 7. Molar fraction at different time.

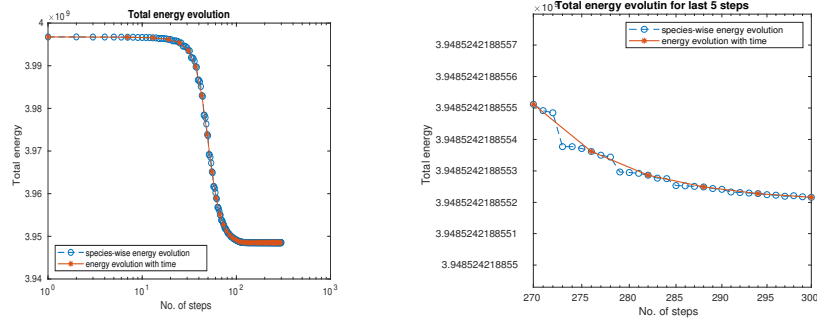


FIGURE 8. Left: Total energy at different time steps; right: zoom-in of total energy at last ten time steps.

Example 5.4. In this example, we apply the proposed numerical scheme to simulate the phase behavior of East Painter reservoir, subject to the gravitational effect [9]. The relevant data and parameters are given in Table 1. The temperature in the reservoir is set as 238K. The computational domain $[0, 1500 \text{ m}]$ is uniformly

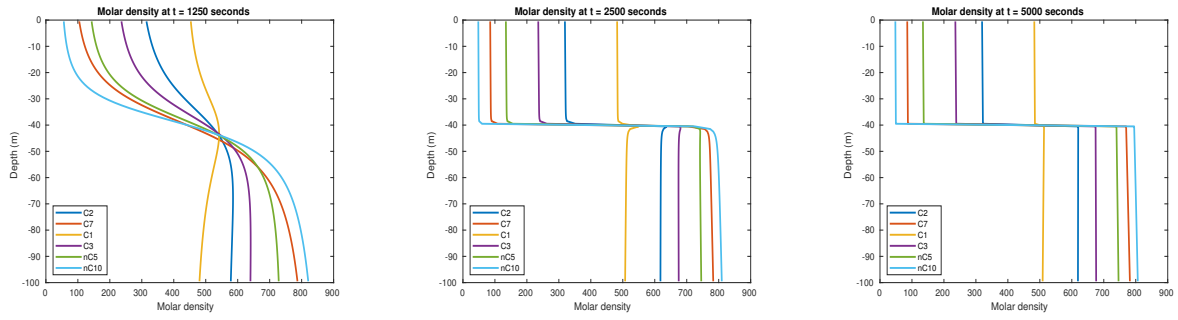


FIGURE 9. Molar density at different time.

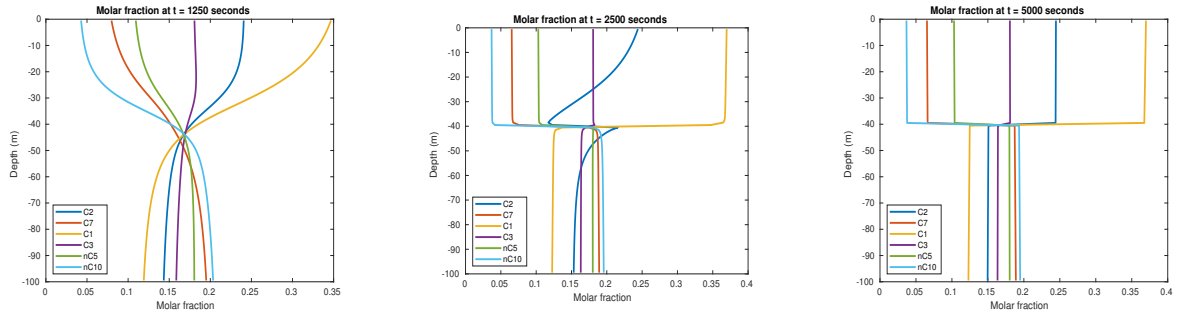


FIGURE 10. Molar fraction at different time.

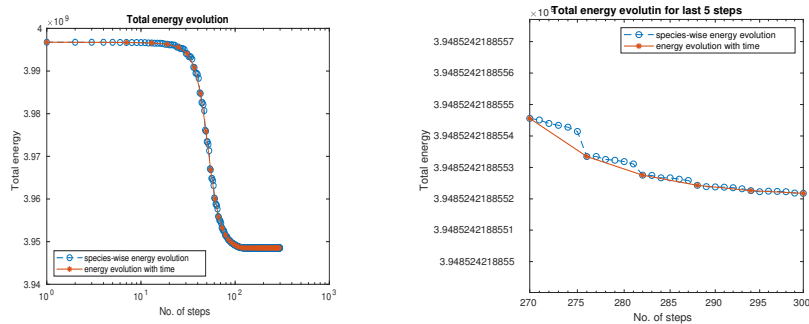


FIGURE 11. Left: Total energy at different time steps; right: zoom-in of total energy at last ten time steps.

split into 500 subintervals. We show the converged molar densities, mole fractions and the molar density in Figure 24 and the total energy changing with time is shown in Figure 25. These results provide some phase behavior properties of East Painter reservoir at the given conditions and further imply the power of the proposed model and numerical schemes.

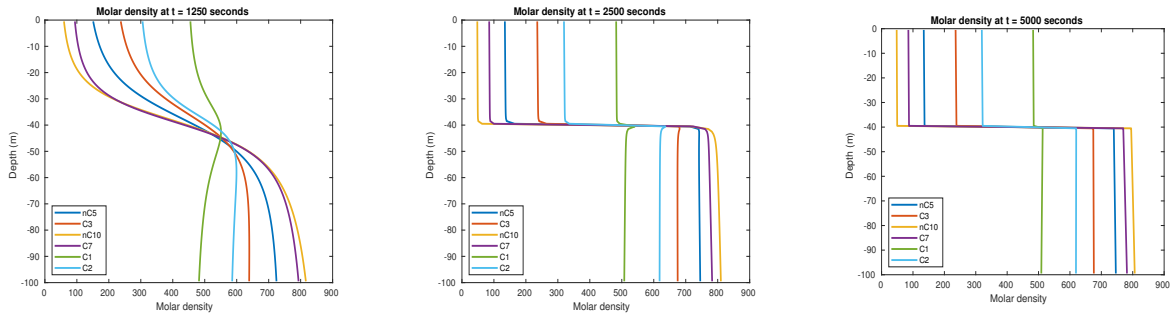


FIGURE 12. Molar density at different time.

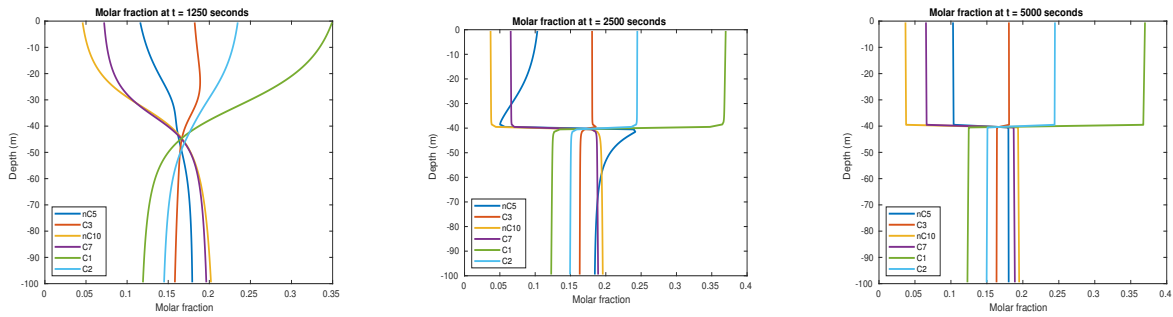


FIGURE 13. Molar fraction at different time.

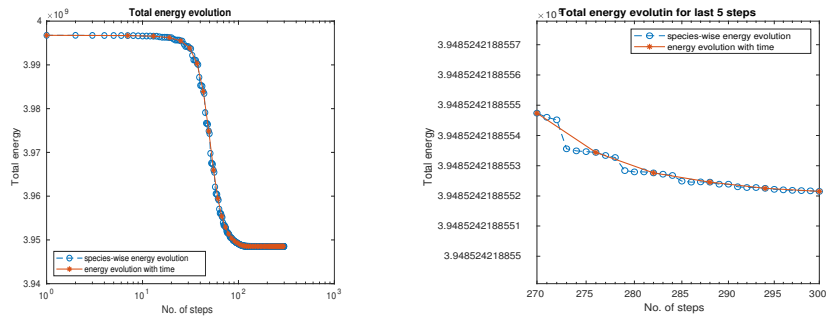


FIGURE 14. Left: Total energy at different time steps; right: zoom-in of total energy at last ten time steps.

CONCLUDING REMARKS

This study has constructed two sets of mathematical models for compositional grading under gravity. One type of the model can be used to model the compositional grading for fluids both in free space and in porous media. The other type of model is derived from the phase equilibrium condition added by a dynamical term to simulate the dynamical processes of composition variation under gravity approaching to an equilibrium state.

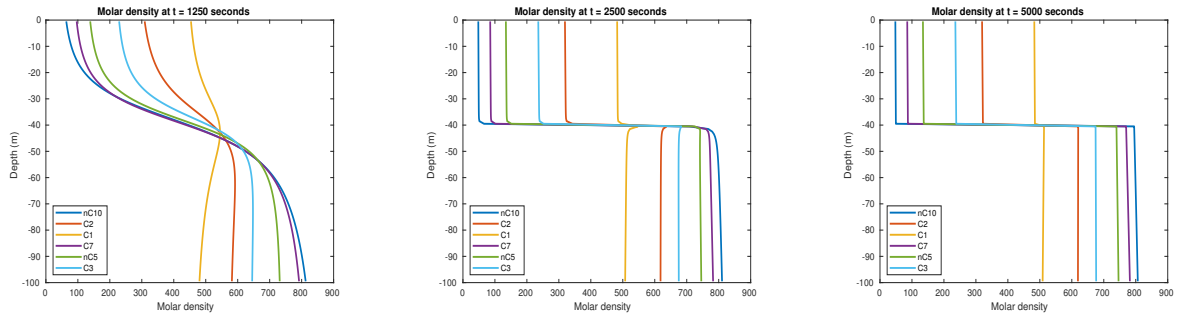


FIGURE 15. Molar density at different time.

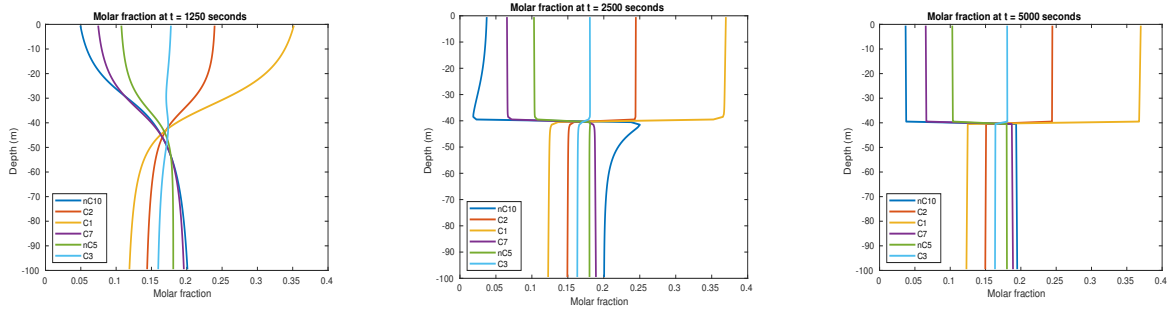


FIGURE 16. Molar fraction at different time.

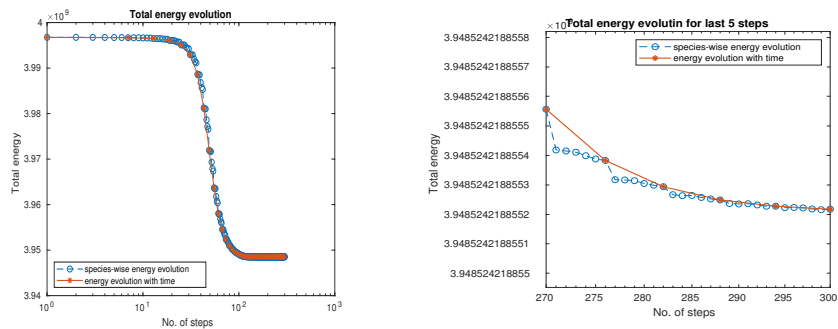


FIGURE 17. Left: Total energy at different time steps; right: zoom-in of total energy at last ten time steps.

An computationally efficient and easy-to-implement numerical scheme for multicomponent fluids is developed. In this scheme only it iteratively solve one nonlinear equation for multicomponent system, which is computationally efficient and reduces the requirement of computer memory when mixture consists of huge number of components. The proposed scheme needs not to choose any special component as reference, which makes the scheme more robust.

Some numerical results are carried out and verify the properties of the scheme. The numerical results are compared with an exact solution for a simplified problem and are matched well.

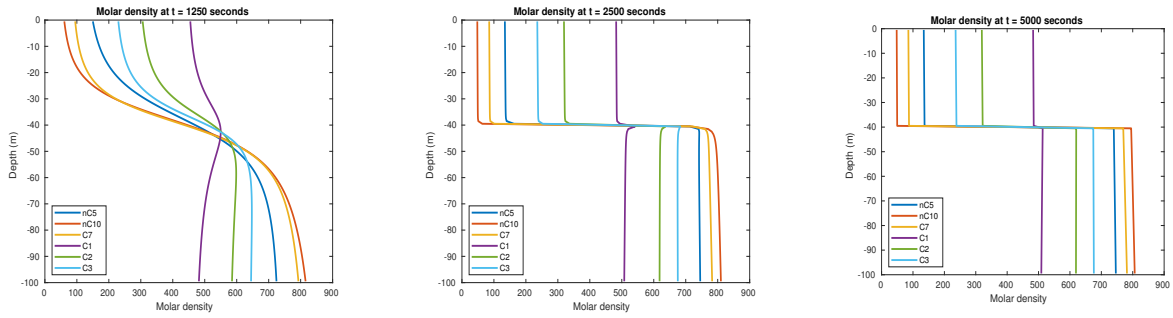


FIGURE 18. Molar density at different time.

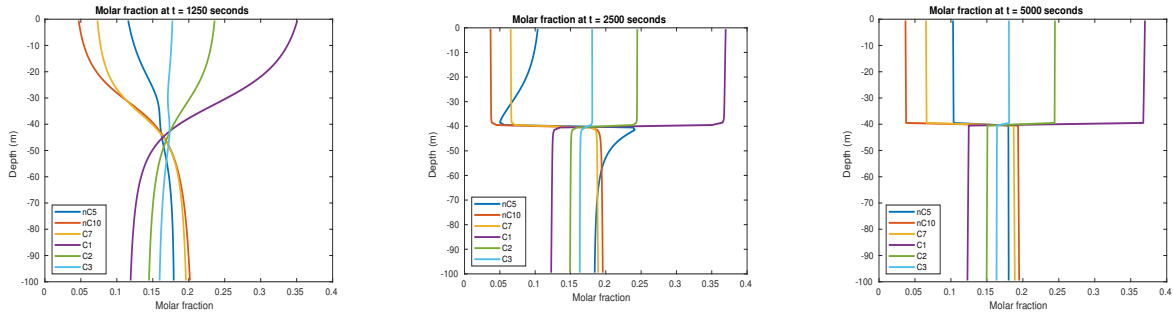


FIGURE 19. Molar fraction at different time.

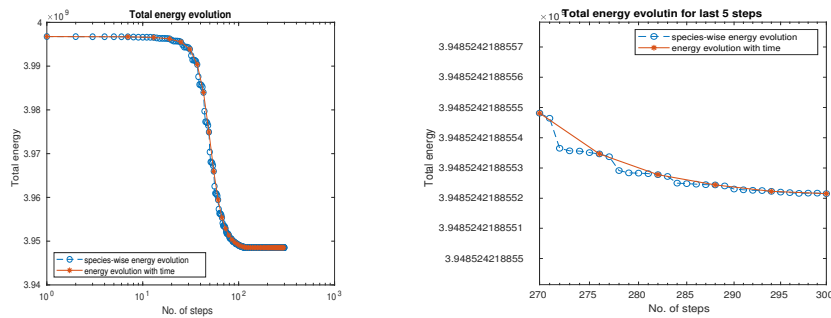


FIGURE 20. Left: Total energy at different time steps; right: zoom-in of total energy at last ten time steps.

ACKNOWLEDGEMENT

Z. Qiao’s work is partially supported by the Hong Kong Research Council GRF grants 15300417 and 15325816 and the Hong Kong Polytechnic University fund G-UAEY. The work of X. Fan and S. Sun is partially supported by King Abdullah University of Science and Technology (KAUST) through the grants BAS/1/1351-01, REP/1/2879-01, and URF/1/3769-01. X. Fan and S. Sun also acknowledge National Natural Science Foundation of China for support (No. 51874262).

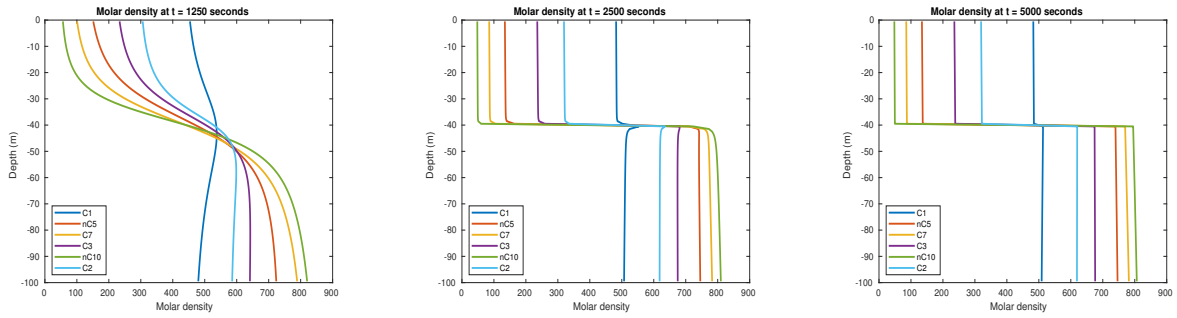


FIGURE 21. Molar density at different time.

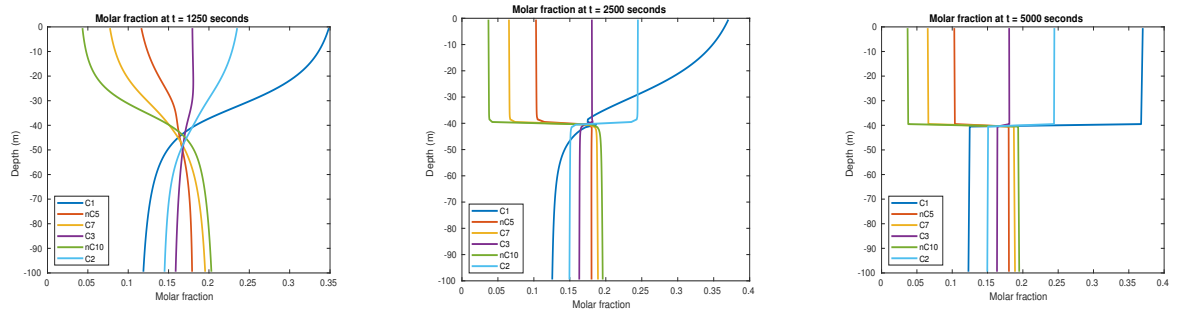


FIGURE 22. Molar fraction at different time.

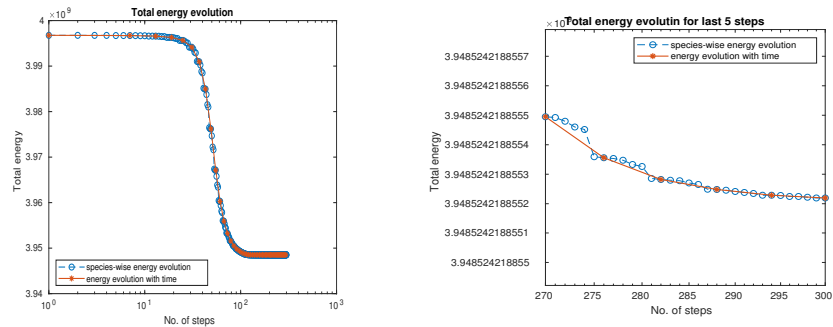


FIGURE 23. Left: Total energy at different time steps; right: zoom-in of total energy at last ten time steps.

APPENDIX A. THE HELMHOLTZ FREE ENERGY DENSITY OF VAN DER WAALS FLUIDS

At constant temperature T , the Helmholtz free energy density as a function of molar density of all species is expressed as the summation of two parts

$$(1.77) \quad f(\mathbf{n}) = f^{\text{ideal}}(\mathbf{n}) + f^{\text{excess}}(\mathbf{n})$$

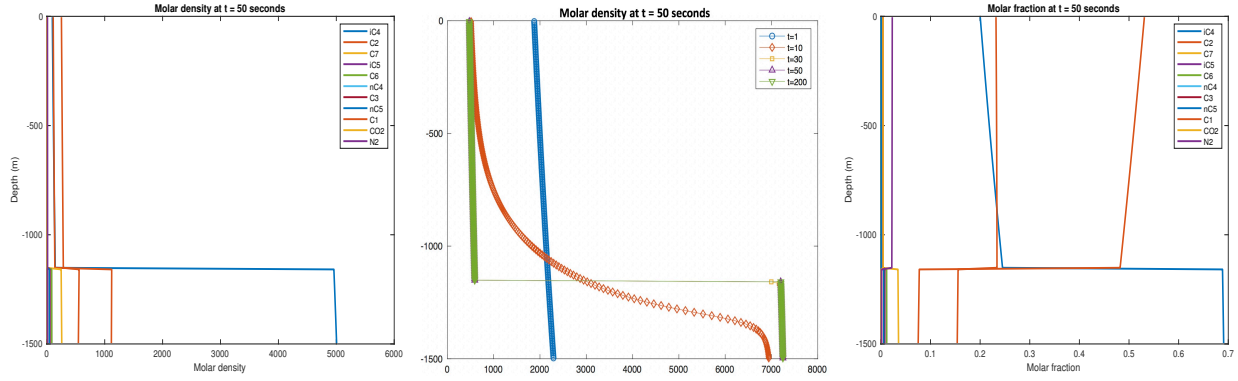


FIGURE 24. Left: molar density; middle: total molar density; right: mole fraction.

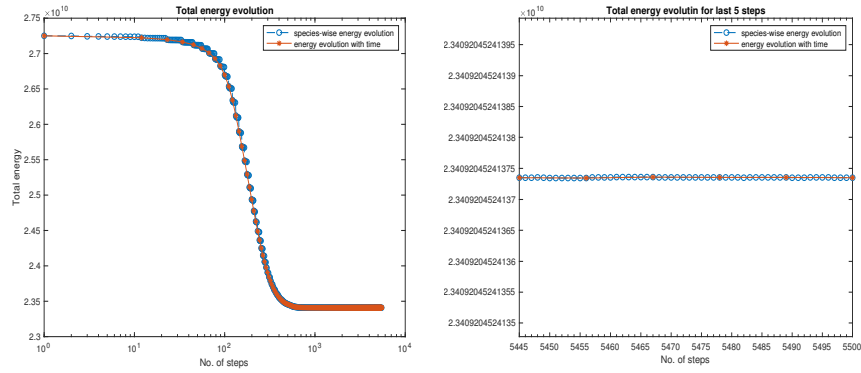


FIGURE 25. Left: Total energy at different time steps; right: zoom-in of total energy at last ten time steps.

where the ideal part $f^{\text{ideal}}(\mathbf{n})$ is given by

$$(1.78) \quad f^{\text{ideal}}(\mathbf{n}) = RT \sum_{i=1}^M n_i (\ln n_i - 1),$$

and the excess term is expressed as

$$(1.79) \quad f^{\text{excess}}(\mathbf{n}) = -RTn \ln(1 - bn) - an^2 = f^b(\mathbf{n}) + f^a(\mathbf{n}).$$

where R is the universal gas constant and

$$(1.80) \quad n = \sum_{i=1}^M n_i,$$

$$(1.81) \quad f^b(\mathbf{n}) = -RTn \ln(1 - bn),$$

$$(1.82) \quad f^a(\mathbf{n}) = RT \sum_{i=1}^M n_i (\ln n_i - 1).$$

For pure-component systems, a and b of the Van der Waals model can be derived from the critical state given as:

$$(1.83) \quad a = \frac{27R^2T_c^2}{64P_c}, \quad b = \frac{RT_c}{8P_c}$$

where P_c and T_c denote the critical pressure and temperature respectively, which can be measured via experiment. For systems of mixture, they are computed by the mixing rules associating with the property of

each component in the mixture:

$$(1.84) \quad a = \sum_{i=1}^M \sum_{j=1}^M x_i x_j (a_i a_j)^{\frac{1}{2}} (1 - k_{ij}), \quad b = \sum_{i=1}^M x_i b_i$$

where a_i and b_i are the parameters for the pure-component Van der Waals parameters computed from (1.83) and x_i is mole fraction of component i given by $x_i = \frac{n_i}{n}$. k_{ij} are the binary interaction coefficients and are obtained from experimental correlation.

Based on the thermodynamics theory, the pressure p of homogeneous fluids is related to the Helmholtz free energy density $f(\mathbf{n})$ by

$$(1.85) \quad p = p(\mathbf{n}, T) = \sum_{i=1}^M n_i \left(\frac{\partial f}{\partial n_i} \right) - f = \sum_{i=1}^M n_i \mu_i - f.$$

Inserting f and μ_i in terms of the Van der Waals model into (1.85) gives

$$p = \frac{nRT}{1 - bn} - an^2.$$

APPENDIX B. THE HELMHOLTZ FREE ENERGY DENSITY OF PENG-ROBINSON FLUIDS

At constant temperature, the Helmholtz free energy density of Peng-Robinson fluids has the same formula of $f^{\text{ideal}}(\mathbf{n})$ and $f^b(\mathbf{n})$ as Van der Waals fluids but different $f^a(\mathbf{n})$ which is given by

$$(2.86) \quad f^a(\mathbf{n}) = \frac{a(T)n}{2\sqrt{2}b} \ln \left(\frac{1 + (1 - \sqrt{2})bn}{1 + (1 + \sqrt{2})bn} \right).$$

For pure-component fluid systems of Peng-Robinson fluids, the parameters $a = a(T)$ and b are respectively given by

$$a = a(T) = 0.45724 \frac{R^2 T_c^2}{P_c} \left(1 + m \left(1 - \sqrt{T_r} \right) \right)^2, \quad b = 0.07780 \frac{RT_c}{P_c},$$

where T_r is reduced temperature defined as $\frac{T}{T_c}$ and all the other parameters except m have the same meanings as in A. The parameter m is a function of the accentric factor ω of the substance formulated by

$$m = 0.37464 + 1.5422\omega - 0.26992\omega^2, \quad \omega \leq 0.49,$$

$$m = 0.379462 + 1.485030\omega - 0.164423\omega^2 + 0.016666\omega^3, \quad \omega > 0.49.$$

The accentric factor is computed by the following formula:

$$\omega = \frac{3}{7} \left(\frac{\log_{10} \left(\frac{P_c}{1 \text{atm}} \right)}{\frac{T_c}{T_b} - 1} \right) - 1,$$

where T_b is the normal boiling point temperature.

For mixtures, $a = a(T)$ and b are computed by the same mixing rule of (1.84).

Expressing f and μ_i in (1.85) in terms of the Peng-Robinson model, we have the following Peng-Robinson equation of state

$$p = \frac{nRT}{1 - bn} - \frac{a(T)n^2}{1 + 2bn - b^2n^2}.$$

REFERENCES

- [1] K. Bao, Y. Shi, S. Sun, and X.P. Wang. A finite element method for the numerical solution of the coupled Cahn–Hilliard and Navie–Stokes system for moving contact line problems. *Journal of Computational Physics*, 231(24):8083–8099, 2012.
- [2] H. Chen, J. Kou, S. Sun, and T. Zhang. Fully mass-conservative IMPES schemes for incompressible two-phase flow in porous media. *Computer Methods in Applied Mechanics and Engineering*, 350:641–663, 2019.
- [3] Z. Chen, G. Huan, and Y. Ma. *Computational methods for multiphase flows in porous media*. SIAM, Philadelphia, 2006.

- [4] C. Dawson, S. Sun, and M. F. Wheeler. Compatible algorithms for coupled flow and transport. *Computer Methods in Applied Mechanics and Engineering*, 193(23):2565–2580, 2004.
- [5] B. Dindoruk and A. Al Kindi. A case study of dynamic modeling of multiple regionally-extensive reservoirs using a unified fluid description. *Journal of Petroleum Science and Engineering*, 78(3):748–758, 2011.
- [6] E. L. Dougherty and H. G. Drickamer. Thermal diffusion and molecular motion in liquids. *The Journal of Physical Chemistry*, 59(5):443–449, 1955.
- [7] H. Elshahawi, M. Hashem, O. C. Mullins, and G. Fujisawa. The missing link—identification of reservoir compartmentalization through downhole fluid analysis. *SPE Annual Technical Conference and Exhibition, Dallas, Texas, October 9–12, 2005*.
- [8] R.H. Espach and J. Fry. Variable characteristics of the oil in the tensleep sandstone reservoir, elk basin field, wyoming and montana. *Petroleum Transactions AIME*, 3(03):75–82.
- [9] R. O. Esposito, P. H.R. Alij, J. A. Scilipoti, and F.W. Tavares. *Compositional Grading in Oil and Gas Reservoirs*. Elsevier, 2017.
- [10] X. Fan, J. Kou, Z. Qiao, and S. Sun. Modeling pore-scale oil-gas systems using gradient theory with peng-robinson equation of state. *Procedia Computer Science*, 80:1364–1373, 2016. International Conference on Computational Science 2016, ICCS 2016, 6-8 June 2016, San Diego, California, USA.
- [11] X. Fan, J. Kou, Z. Qiao, and S. Sun. A componentwise convex splitting scheme for diffuse interface models with van der waals and Peng–Robinson equations of state. *SIAM Journal on Scientific Computing*, 39(1):B1–B28, 2017.
- [12] A. Firoozabadi, K. Ghorayeb, and K. Shukla. Theoretical model of thermal diffusion factors in multicomponent mixtures. *AIChE J.*, 46(5):892–900, 2000.
- [13] J. W. Gibbs. *The Scientific Papers of J.W. Gibbs Vol. 1*. Dover Publications, New York, 1961.
- [14] A. Gibson, H. Srensen, M. Abdou, and Sener. New methods for the nonequilibrium initialization of reservoir models with lateral and vertical variations in the initial fluid composition. *SPE Petroleum Exhibition and Conference, Abu Dhabi, U.A.E., November 5–8, 2006*.
- [15] A. Hirschberg. Role of asphaltenes in compositional grading of a reservoir’s fluid column. *Journal of Petroleum Technology*, 40(01):89–94, 1980.
- [16] L. Hoier and C. H. Whitson. Compositional grading—theory and practice. *SPE Reservoir Evaluation & Engineering*, 4(06):525–535, 2000.
- [17] T. Jindrova and J. Mikyska. General algorithm for multiphase equilibria calculation at given volume, temperature, and moles. *Fluid Phase Equilibria*, 393:7–25, 2015.
- [18] M. Kiani, S. Osfouri, R. Azin, and S. A. M. Dehghani. Impact of fluid characterization on compositional gradient in a volatile oil reservoir. *Journal of Petroleum Exploration and Production Technology*, 6(4):835–844, 2016.
- [19] J. Kou and S. Sun. Multi-scale diffuse interface modeling of multi-component two-phase flow with partial miscibility. *Journal of Computational Physics*, 318:349–372, 2016.
- [20] J. Kou and S. Sun. Efficient energy-stable dynamic modeling of compositional grading. *International Journal of Numerical Analysis and Modeling*, 14:218–242, 2017.
- [21] J. Kou and S. Sun. A stable algorithm for calculating phase equilibria with capillarity at specified moles, volume and temperature using a dynamic model. *Fluid Phase Equilibria*, 456:7–24, 2018.
- [22] J. Kou and S. Sun. Thermodynamically consistent modeling and simulation of multi-component two-phase flow with partial miscibility. *Computer Methods in Applied Mechanics and Engineering*, 331:623–649, 2018.
- [23] J. Kou, S. Sun, and X. Wang. An energy stable evolution method for simulating two-phase equilibria of multi-component fluids at constant moles, volume and temperature. *Computational Geosciences*, 20(1):283–295, 2016.
- [24] J. Kou, S. Sun, and X. Wang. Linearly decoupled energy-stable numerical methods for multicomponent two-phase compressible flow. *SIAM Journal on Numerical Analysis*, 56(6):3219–3248, 2018.
- [25] Jisheng Kou, Shuyu Sun, and Xiuhua Wang. A novel energy factorization approach for the diffuse-interface model with peng-robinson equation of state. *SIAM Journal on Scientific Computing*, 42(1):B30B56, 2020.
- [26] T. LaForce and R. T. Johns. Effect of initial gas saturation on miscible gasflood recovery. *Journal of Petroleum Science and Engineering*, 70(3):198–203, 2010.

- [27] S. T. Lee. Capillary-gravity equilibria for hydrocarbon fluids. *SPE Paper 19650. 1989 SPE 64th Annual Technical Conference and Exhibition, San Antonio, Texas, October 8–11.*
- [28] G.N. Lewis and M. Randall. *Thermodynamics and the Free Energy of Chemical Substances.* McGraw–Hill, New York, 1923.
- [29] Y. Li, J. Kou, and S. Sun. Numerical modeling of isothermal compositional grading by convex splitting methods. *Journal of Natural Gas Science and Engineering*, 43:207–221, 2017.
- [30] Y. Li, T. Zhang, S. Sun, and X. Gao. Accelerating flash calculation through deep learning methods. *Journal of Computational Physics*, 394:153–165, 2019.
- [31] C. Lira-Galeana, A. Firoozabadi, and J. M. Prausnitz. Computation of compositional grading in hydrocarbon reservoirs application of continuous thermodynamics. *Fluid Phase Equilibria*, 102(2):143–158, 1994.
- [32] D.R. McCord. Performance predictions incorporating gravity drainage and gas cap pressure maintenance—ll-370 area, bolivar coastal field. *Petroleum Transactions AIME*, 5(09):231–248.
- [33] J. Mikyška and A. Firoozabadi. A new thermodynamic function for phase-splitting at constant temperature, moles, and volume. *AIChE Journal*, 57, 2011.
- [34] M. R. Moldover, J. V. Sengers, R.W. Gammon, and R. J. Hocken. Gravity effects in fluids near the gas–liquid critical point. *Review of Modern Physics*, 51(1):79–101.
- [35] F. Montel and P.L. Gouel. Prediction of compositional grading in a reservoir fluid column. *SPE Annual Technical Conference and Exhibition*, pages 22–25, 1985.
- [36] Francois Montel, Jacques Bickert, Aurilie Lagisquet, and Guillaume Galliro. Initial state of petroleum reservoirs: A comprehensive approach. *Journal of Petroleum Science and Engineering*, 58(3):391–402, 2007.
- [37] M. Muskat. Distribution of non-reacting fluids in the gravitational field. *Phys. Rev.*, 35:1384–1393, 1930.
- [38] M. H. Nikpoor and Z. Chen. New methodology for the modeling of compositional grading within the gas–oil transition zone in petroleum reservoirs. *Energy Sources, Part A: Recovery, Utilization, and Environmental Effects*, 35(5):438–444, 2013.
- [39] M. H. Nikpoor, M. Dejam, Z. Chen, and M. Clarke. Chemicalgravitythermal diffusion equilibrium in two-phase non-isothermal petroleum reservoirs. *Energy & Fuels*, 30(3):2021–2034, 2016.
- [40] M. H. Nikpoor, R. Kharrat, and Z. Chen. Modeling of compositional grading and plus fraction properties changes with depth in petroleum reservoirs. *Petroleum Science and Technology*, 29(9):914–923, 2011.
- [41] O Obidi, AH Muggeridge, and V Vesovic. Analytical solution for compositional profile driven by gravitational segregation and diffusion. *Physical Review E*, 95(2):022138, 2017.
- [42] O. C. Obidi. *Timescales for the Development of Thermodynamic Equilibrium in Hydrocarbon Reservoirs.* PhD thesis, 2014.
- [43] K.G.O. Padua. Nonisothermal gravitational equilibrium model. *PE Reservoir Evaluation & Engineering*, 2(02):211–217, 1999.
- [44] O. Polvka and J. Mikyka. Compositional modeling in porous media using constant volume flash and flux computation without the need for phase identification. *Journal of Computational Physics*, 272:149–169, 2014.
- [45] Z. Qiao and S. Sun. Two-phase fluid simulation using a diffuse interface model with Peng–Robinson equation of state. *SIAM Journal on Scientific Computing*, 36(4):B708–B728, 2014.
- [46] Z. Qiao, S. Sun, T. Zhang, and Y. Zhang. A new multi-component diffuse interface model with Peng–Robinson equation of state and its scalar auxiliary variable (SAV) approach. *Communications in Computational Physics*, 26(5):1597–1616, 2019.
- [47] Z. Qiao, X. Yang, and Y. Zhang. Thermodynamic-consistent multiple-relaxation-time lattice boltzmann equation model for two-phase hydrocarbon fluids with peng-robinson equation of state. *International Journal of Heat and Mass Transfer*, 141:1216–1226, 2019.
- [48] W.G. Riemens, A.M. Schulte, and L.N.J. de Jong. Birba field pvt variations along the hydrocarbon column and confirmatory field tests. *Journal of Petroleum Technology*, 40(01):83–88, 1988.
- [49] B.H. Sage and W.N. Lacey. Gravitational concentration gradients in static columns of hydrocarbon fluids. *Petr. Trans. AIME*, 132(01):120–131, 1939.

- [50] A.M. Schulte. Compositional variations within a hydrocarbon column due to gravity. *SPE Annual Technical Conference and Exhibition, 21-24 September, Dallas, Texas*, pages 21–24, 1980.
- [51] P. C. Smalley and W. A. England. Assessing reservoir compartmentalization during field appraisal: How geochemistry can help. *SPE European Petroleum Conference*.
- [52] S. Sun. Darcy–scale phase equilibrium modeling with gravity and capillarity. *Journal of Computational Physics*, 399:108908, 2019.
- [53] K. O. Temeng, M. J. Al-Sadeg, and A. Al-Mulhim. Compositional grading in the ghawar khuff reservoirs. *SPE Annual Technical Conference and Exhibition, New Orleans, Louisiana, September 27–30, 1998*.
- [54] R. J. Wheaton. Treatment of variation of composition with depth in gas-condensate reservoir. *SPE Reserv. Eng.*, 6(02):239–244, 1991.
- [55] H. Yang, S. Sun, Y. Li, and C. Yang. A fully implicit constraint–preserving simulator for the black oil model of petroleum reservoirs. *Journal of Computational Physics*, 396:347–363, 2019.
- [56] G. Zhu, J. Kou, B. Yao, Y.-S. Wu, J. Yao, and S. Sun. Thermodynamically consistent modelling of two–phase flows with moving contact line and soluble surfactants. *Journal of Fluid Mechanics*, 879:327–359, 2019.

(X. Fan) SCHOOL OF MATHEMATICAL SCIENCES, GUIZHOU NORMAL UNIVERSITY, GUIYANG, P. R. CHINA
E-mail address: scixlf@163.com, xiaolin.fan@kaust.edu.sa

(Z. Qiao) DEPARTMENT OF APPLIED MATHEMATICS, THE HONG KONG POLYTECHNIC UNIVERSITY, HUNG HOM, HONG KONG
E-mail address: zhonghua.qiao@polyu.edu.hk

(S. Sun) KING ABDULLAH UNIVERSITY OF SCIENCE AND TECHNOLOGY (KAUST), PHYSICAL SCIENCE AND ENGINEERING (PSE), THUWAL 23955-6900, SAUDI ARABIA
E-mail address: shuyu.sun@kaust.edu.sa